J Plant Growth Regul (2006) 25:313–323
DOI: 10.1007/s00344-006-0067-9

J P G R
Journal of Plant Growth Regulation

The Possible and the Actual in Phyllotaxis: Bridging the Gap between Empirical Observations and Iterative Models

Scott Hotton,[1,3] Valerie Johnson,[2] Jessica Wilbarger,[2] Kajetan Zwieniecki,[3] Pau Atela,[2] Christophe Golé,[2] and Jacques Dumais[3]*

[1]*UC Merced Center for Computational Biology, University of California, Merced, California 95344, USA;* [2]*Department of Mathematics, Smith College, Northampton, Massachusetts 01063, USA;* [3]*Department of Organismic and Evolutionary Biology, Harvard University, Cambridge, Massachusetts 02138, USA*

Abstract

This article presents new methods for the geometrical analysis of phyllotactic patterns and their comparison with patterns produced by simple, discrete dynamical systems. We introduce the concept of ontogenetic graph as a parsimonious and mechanistically relevant representation of a pattern. The ontogenetic graph is extracted from the local geometry of the pattern and does not impose large-scale regularity on it as for the divergence angle and other classical descriptors. We exemplify our approach by analyzing the phyllotaxis of two asteraceae inflorescences in the light of a hard disk model. The simulated patterns offer a very good match to the observed patterns for over 150 iterations of the model.

Key words: Artichoke; Delaunay triangulation; Dynamical system; Shoot apical meristem; Phyllotaxis; Sunflower; Voronoi tessellation

Introduction

Numerous patterns in nature are made of identical units repeated regularly in space. Microtubules and viral capsids provide examples at the molecular level (Erickson 1973). Given that proteins and other macromolecules assemble over length scales that are only slightly larger than those of inorganic crystals, it is not overly surprising that they offer patterns of similar regularity. However, when crystal-like regularity is found at the level of an entire living organism, one may justly be astonished. Yet, this is a common occurrence in plants where the arrangement of leaves and flowers around the stem, known as phyllotaxis, yields striking patterns (Figure 1).

The symmetries found in crystals, biopolymers, and plants reflect two simple geometrical rules: (1) equivalent or nearly equivalent units are added in succession and (2) the position of new units is determined by interactions with the units already in

Received: 26 June 2006; accepted: 29 June 2006; Online publication: 30 November 2006
*Corresponding author; e-mail: jdumais@oeb.harvard.edu

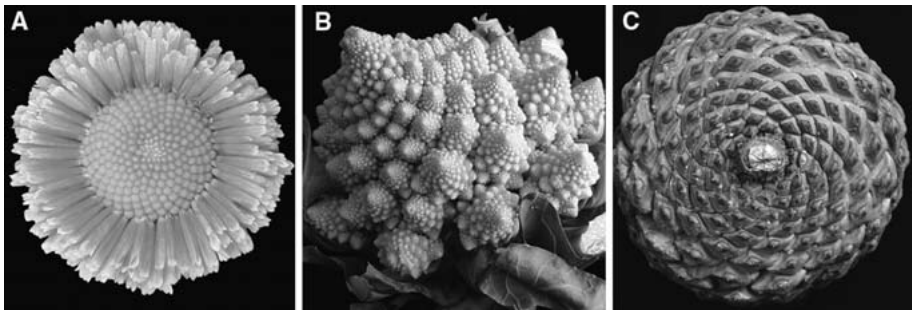

Figure 1. Crystal-like patterns in plants. (**A**) *Bellis perennis*, (**B**) broccoli romanesco (*Brassica oleracea*), (**C**) pine cone (*Pinus sp*).

place. To visualize these rules in plants, one must focus on the shoot apical meristem where leaf and flower primordia are initiated in a stereotypical manner. Experimental evidence suggests that primordium initiation is possible only in the peripheral region of the meristem (Reinhardt and others 2000, 2003b). Moreover, within that region, older primordia are thought to exert an inhibitory effect on primordium initiation (Snow and Snow 1932; Reinhardt and others 2003a). A new primordium thus forms in the largest gap available within the peripheral region. Repetition of this process leads, at the global scale, to the emergence of two families of spirals called parastichies (these two families are particularly clear in Figure 1C). The numbers of parastichies in these two families are often consecutive Fibonacci numbers (1, 1, 2, 3, 5, 8, 13, ...). The divergence angle between consecutive primordia is often close to the golden angle $\alpha = 360(2 - \tau)^\circ \approx 137.5^\circ$, where $\tau \approx 1.608$ is the golden mean (Figure 2).

Perhaps the most astonishing observation about phyllotaxis is the narrow range of patterns reported across all major groups of vascular plants. This observation is the basis of one of the oldest questions in plant biology: why, of all the possible patterns that can be created by repeating identical units in space, is only a rather small set ever seen in plants? This question presents a formidable challenge because it presupposes some formal understanding of what patterns are possible whether or not these patterns are observed in nature. One approach to answering this question is to develop the simplest model of phyllotaxis that can reproduce the classic patterns found in plants. Comparison between the model and observed patterns can help establish what features of the model are sufficient to account for phyllotaxis. Moreover, if the model remains simple, it should be possible to perform a complete study of its morphogenetic potential, thus pinpointing the necessary conditions required to generate the class of patterns observed in nature.

In this article we focus on the first aspect of this problem and attempt to bridge the gap between

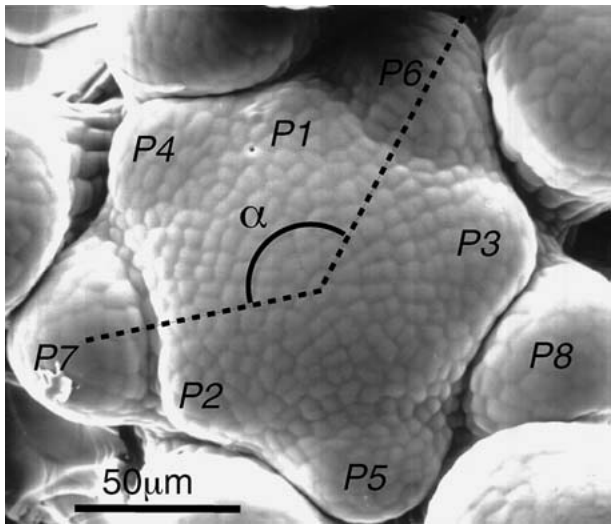

Figure 2. Primordium initiation at the shoot apical meristem of *Arabidopsis thaliana*. Flower primordia are numbered according to their order of initiation. Note the constant divergence angle (α) between primordia.

observed phyllotactic patterns and simple geometrical models. The bridge rests on three pillars:

1. a protocol to extract precise quantitative information from meristem images.
2. a dynamical system model that can reproduce observed phyllotactic patterns.
3. a new concept, the ontogenetic graph, that provides the basis for comparing observed and simulated phyllotactic patterns.

This article is organized around these three contributions. For clarity, we discuss only patterns on a disk, although our approach encompasses the whole breadth of phyllotactic patterns found in plants.

Dynamical Geometric Models of Phyllotaxis

The classical geometric models of phyllotaxis all refer to lattices—either helices on a cylinder or

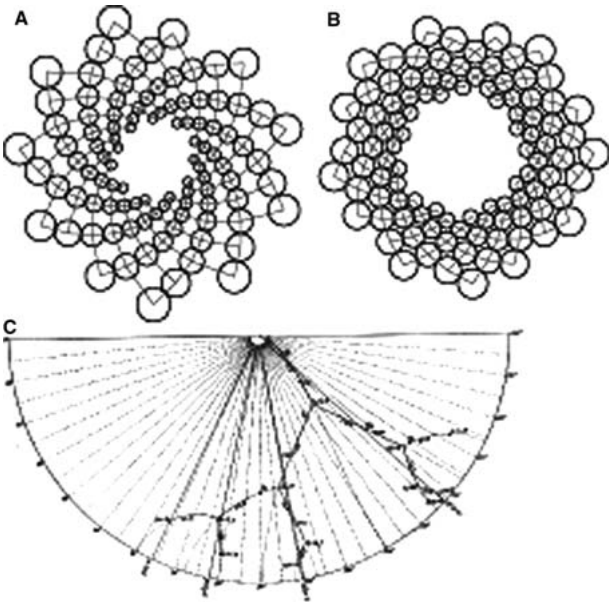

Figure 3. (**A**) A spiral lattice with parastichy numbers 11, 20. This pattern is not a phyllotactic lattice as only one parastichy family can be formed with tangent disks. (**B**) A phyllotactic lattice, with parastichy numbers 13, 21. (**C**) The space of all spiral lattice as drawn by van Iterson in 1907. The tree structure is the subset of lattices corresponding to the type of phyllotactic patterns observed in nature.

spirals on a disk. A spiral lattice is a set of points $P_k = (\rho^k, k\alpha)$, where α is the divergence angle, ρ is the plastochrone ratio (that is, the ratio of the radial distances for two successive primordia), and k is any integer between zero and infinity. The curve that joins the lattice points ordered by k is called the *ontogenetic spiral*. The visible spirals in these patterns, joining each point to its nearest neighbors, are called *parastichies* (Figure 3). Not all lattices are similar to the patterns exhibited by plants. The so-called phyllotactic lattices are represented by a collection of disks centered at the lattice points such that they are tangent along two families of parastichies winding in opposite directions from each other (compare Figure 3A and 3B). The set of parameters (ρ, α) yielding phyllotactic lattices was studied by van Iterson (1907) (Figure 3C) and forms a tree structure within the much larger space of all lattices. van Iterson's work represents the first attempt to interprete phyllotactic patterns in the context of a wider space of patterns (here lattices).

Dynamical Models of Phyllotaxis

Although much has been learned from the study of lattices (Bravais and Bravais 1837; van Iterson 1907; Levitov 1991; Adler 1998), they are lacking in one important aspect: in lattices, the location of primordia is preset, and therefore they fail to account for the second developmental rule, which stipulates that primordium position is determined by interactions with primordia already in place. The preset position is at variance with experimental observations that patterns build on previous patterns. In this article, we use a geometric dynamical systems approach that builds on a previous model by Atela and others (2002). We were inspired by the iterative models of Douady and Couder (1996) (see also the related systems proposed by Williams and Brittain 1984; Schwabe and Clewer 1984; Kunz 1997; Koch and others 1998; d'Ovidio and Mosekilde 2000).

These dynamical system models are implementations of the two rules stated in the introduction, as applied to phyllotaxis. More specifically:

1. Primordia are formed in succession, one or more at a time.
2. Primordia are positioned in the ''least crowded spot'' at the edge of the meristem.

If one assumes that primordia form with fixed period, one obtains what Douady and Couder called the *Hofmeister hypothesis*. If one assumes that new primordia form *when* and *where* there is enough space, one obtains the so-called *Snow hypothesis*. The Snow hypothesis has the advantage of allowing simultaneous formation of several primordia (sometimes yielding multijugate configurations). Several reports have established that these dynamical systems can reproduce many features of the van Iterson diagram (Douady and Couder 1996; Kunz 1997; Koch and others 1998; d'Ovidio and Mosekilde 2000; Atela and others 2002).

Mathematically, these models can be seen as discrete dynamical systems acting on points $(R_0, \theta_0), \cdots, (R_N, \theta_N)$ of the disk (each point representing the center of a primordium in polar coordinates) with a transformation from one configuration to the next of the form:

$$(R_0, \theta_0, \ldots, R_N, \theta_N) \rightarrow (f(R_0, \theta_0, \ldots, R_N, \theta_N), R_0, \theta_0, \ldots, R_{N-1}, \theta_{N-1}),$$

where the function f determines the location of the new primordium that minimizes its interaction with the existing ones. In other words, f expresses the location *and* time at which the interaction W falls below a certain threshold. Most authors consider an interaction of the form

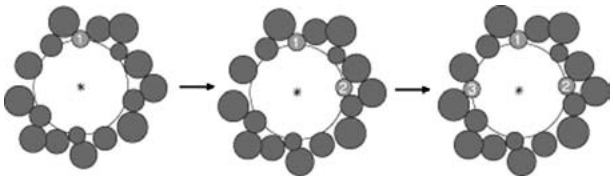

Figure 4. Three iterates of the Snow transformation.

$$W(R, \theta, R_0, \theta_0, \ldots, R_N, \theta_N) = \sum_k u(R, \theta, R_k, \theta_k),$$

where (R,θ) is the test location of the new primordium and u is a more or less explicit function of the distance between (R_k,θ_k) and (R,θ). Douady and Couder used, among others, $u = c/dist^a$, where a and c are constants and *dist* is the distance between (R_k,θ_k) and (R,θ).

The Hard Disk Limit

An important aspect of the dynamical systems is the nature of the interaction W and, in particular, the set of primordia directly involved in determining the location of new primordia. Some of us have proposed (Atela and others 2002; Atela and Golé 2006) a radical simplification of the interaction as

$$W^*(R, \theta, R_0, \theta_0, \ldots, R_{N,}\theta_N) = \max_k u(R, \theta, R_k, \theta_k).$$

In other words, we neglect all but the largest interaction; equivalently, *we assume that a new primordium only feels its closest neighbor*. This limit is sometimes called the ''hard disk limit.''

The hard disk limit is in fact inspired from experimental observations. Ablation experiments have shown that only the set of most recently formed primordia around the circumference of the meristem plays a role in determining the position of the next primodium (Snow and Snow 1932; Reinhardt and others 2003a). Moreover, the two primordia directly contacting a newly formed primordium help determine its size (Reinhardt and others 2003a).

In this article we use the hard disk Snow model. Our goal in defining dynamical models of primordia formation is to reproduce phyllotactic patterns with the simplest model possible. We assume that primordia are small disks placed around a larger disk that simulates the meristem. Given a configuration of primordia, a new primordium appears in the place that is farthest away from the center of the meristem. This condition is equivalent to minimizing a potential where only the contribution of the closest primordium is felt (that is, fast decay of the potential). The process is then iterated again and again (Figure 4).

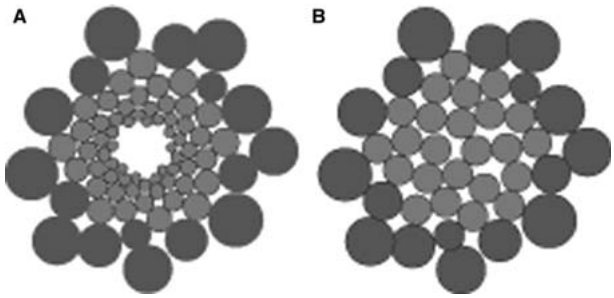

Figure 5. Two modes of growth with the same initial condition (in dark gray) derived from a micrograph of *Picea abies*. (**A**) The constant ratio model (Γ = 0.176 on a unit radius meristem) yields a pattern which, although not a lattice, does exhibit families of spirals that are parastichy like, with parastichy numbers 8, 13 – which are indeed the parastichy numbers of the original pattern. (**B**) The same initial condition yields a very different pattern with the constant radius model (r = 0.176).

Experimental observations support two qualitatively different classes of models (Figure 5):

The *constant ratio model* assumes that the ratio Γ of the new primordium radius over the meristem radius remains constant. After each iteration, the configuration of existing primordia (along with their radii) expands uniformly away from the center until there is enough room on the edge of the meristem for a new primordium. This mode of growth can be sustained indefinitely: primordia never fill the meristem. It is observed in most indeterminate meristems and also at intermediate stages of capitulum development in sunflowers when the growth of the meristem is balanced by the progression of the morphogenetic front of primordia (Palmer and Steer 1985). Only this mode can generate spiral lattices, which appear as steady states for this model (for example, the [13, 21] lattice in Figure 3B is such a steady state).

The *constant radius model* assumes that new primordia are formed with constant radius and that the meristem does not grow at all. As a consequence, the primordia fill up the center of the meristem. This has been observed to be approximately the case in the very latest stage of capitulum development in sunflowers (Palmer and Steer 1985).

These models are just two notable elements in a continuum of models in which the ratio parameter varies with the distance to the center at various rates. This is not the place to provide a complete analysis of these models. See Atela and others (2002) and Douady (1998) for a complete and rigorous

mathematical analysis of the bifurcation diagram using the hard disk assumption in the cylinder.

Materials and Methods

The experimental protocol was designed with two goals in mind. First, we strive to observe phyllotactic patterns as they develop. This precaution is necessary because plant patterns can be altered substantially by the growth that follows their establishment. Second, we have tried to select meristems with simple geometry and a relatively complex phyllotaxis. The inflorescences of asteraceae are ideal in that respect. We have therefore selected one sunflower (*Helianthus annuus*) capitulum and one artichoke (*Cynara scolymus*) capitulum to illustrate our approach.

Replica Technique

Observation of developing phyllotactic patterns was based on a nondestructive replica technique (Williams and Green 1988; Dumais and Kwiatkowska 2002; Kwiatkowska and Dumais 2003). An impression polymer (GC EXAFLEX, G-C Dental Industrial Corp., Tokyo, Japan) was used to obtain accurate molds of the meristem surface at different time points. These molds were filled with epoxy resin (Ace Hardware Corp. Illinois), and the resulting casts were imaged in a scanning electron microscope.

Meristem Reconstructions

Three-dimensional reconstructions are required to characterize the geometry of the meristem surface and to determine precisely the position of primordia. The stereoscopic techniques and computational tools used to make 3-D reconstructions have already been described in detail by Dumais and Kwiatkowska (2002). Surface reconstructions were based on stereoimages of the same meristem taken from slightly different viewpoints (10° tilt angle). We used area matching to find corresponding points on the two stereoimages. We first overlaid a grid onto one of the stereoimages, which hereafter will be referred to as the ''reference image.'' For each grid vertex on the reference image, we searched the target meristem image for a matching area. The match was based on a window of 25 × 25 pixels (for comparison, the diameter of a floret in Figure 6 is about 100 pixels) and was quantified with the cross-correlation coefficient between the pixel intensities of the reference and target areas (Hein and others 1999).

The inputs for the stereoscopic reconstruction are two matrices specifying the 2-D position of corresponding vertices on the stereoimages. The 3-D coordinates are given by: $x = (x_a + x_b)/2m$, $y = (y_a + y_b)/2m\cos(\gamma/2)$, and $z = (y_a - y_b)/2m\sin(\gamma/2)$, where γ is the tilt angle about the x axis, $(x_a, y_a)$and (x_b, y_b) are the vertex coordinates before and after tilting, and m is the magnification (Piazzesi 1973).

Collection of Primordia Centers and Their Triangulation

To assist with data collection and management, computer tools were developed and implemented in MATLAB (The Mathworks, Natick, MA). Coordinates for primordia were obtained from digital scanning electron micrographs. The corresponding *x,y,z* coordinates were found by mapping to the reconstructed surface. The location of primordia must be complemented by information about the contacts between primordia. The procedure used to identify such contacts was based on Voronoi cells (also called *Dirichlet domains*). Voronoi cells were previously applied to the study of phyllotactic patterns (Rothen and Koch 1989; Rivier and others 1984). Given a set of primordium positions P_1, P_2, ..., P_N , in the plane, the Voronoi cell of P_i consists of all the points in the plane that are closer to P_i than to any other point P_k.

Connecting the centers of adjacent Voronoi cells by line segments produces the Delaunay triangulation for the configuration. The Delaunay triangulation is dual to the Voronoi diagram and contains the same information. In particular, the adjacency relationships between primordia are represented by the edges of the Delaunay triangulation. The Delaunay data were used to draw, in each Voronoi cell, a circle centered at the center of the cell, and tangent to its closest edge. We call this circle the *Voronoi inscribed circle*. We have used the Voronoi inscribed circles as approximations to primordia, keeping in mind that, in general, they slightly underestimate the actual sizes of primordia.

Implementation of Dynamical Systems

The programs for the two dynamical system models were written in MATLAB. Given a configuration of disks, we compute all the possible children of the existing primordia—that is, all the disks tangent to a pair of existing disks and located inward. These candidate children are weeded out if they overlapped with existing primordia, and the one farthest from the center was chosen as the new primordium.

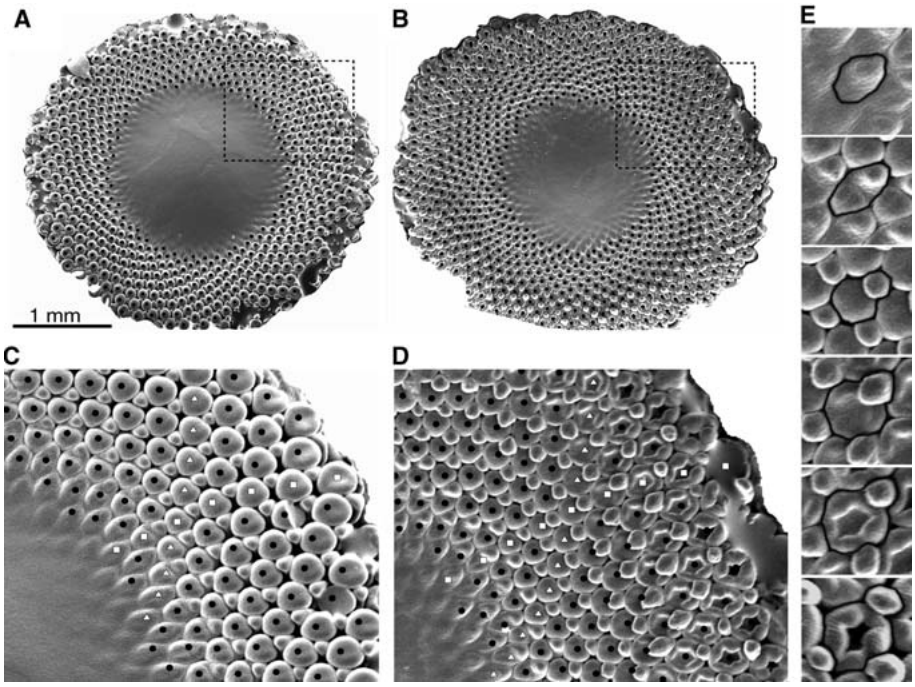

Figure 6. Sequential replicas of the sunflower capitulum. (**A**) and (**B**) Epoxy casts of the same capitulum collected two days apart. (**C**) and (**D**) Close-ups showing the development of the parastichies on the capitulum. Note that some of the flower primordia are replaced by voids corresponding to air bubbles trapped in the epoxy cast. (**E**) Typical primordium development. The flower bract (upper right structure in each panel) appears first and is followed by the development of the disk floret.

The constant ratio model has the added complication that the correct ratio must be chosen. To do so, the program first chooses a candidate of reasonable radius (for example, the radius of the last primordium); it then solves an equation of degree four to find the center of the primordium tangent to the same parents, but with the radius r that yields the correct ratio Γ. A new search of candidates is performed with disks of radius r to check whether the change of radius might have yielded another possible location farther away from the center. Resizing is performed once again. We have never observed a case where this bootstrap process needed more than two rounds of candidate search.

As Figure 5 shows, only one layer of primordia is enough to determine the development of the pattern. Therefore, to simulate observed patterns, we first selected as initial conditions a ring of primordia given by the plant data at hand. We call this ring of primordia a *primordia front*. To find fronts, we wrote a MATLAB program allowing the user to interactively pick a primordium P_0 on a micrograph. The program then finds the closest data point (recorded as center of the primordium) and computes its distance to the meristem center. Each successive point of the front is then chosen as child or parent of the previous one, in such a way that its distance to the center is as small as possible without being closer to the center than P_0. The process stops when a primordium adjacent to P_0 is reached, thus closing the loop.

Results

Time Sequences and Stereoscopic Reconstructions

Several experimental approaches have been developed to observe meristem growth and primordium initiation over time (Dumais and Kwiatkowska 2002; Grandjean and others 2004; Reddy and others 2004). Here we adopt a replica technique because of its flexibility and ease of use. Figure 6 shows two replicas of a sunflower capitulum taken at a 2-day interval. During this interval, approximately two new primordia were generated along the steep parastichies (squares in Figure 6C and 6D) and three along the shallow parastichies (triangles in Figure 6C and 6D). Inspection of Figure 6A and 6B reveals that the development of the pattern has been accommodated in part by an outward displacement of older flowers and by a short advance of the pattern into the central unpatterned region. Because the central region has been reduced slightly, we can conclude that the development departs from the constant ratio model described above. However, given the large size of the morphogenetic region compared to the size of the newly formed primordia, the deviation is likely to be negligible.

Figure 7 shows a reconstructed sunflower capitulum. The level of contrast in the unpatterned central region was too low to allow reliable

reconstruction; it was therefore excluded. From the reconstruction, it is possible to find a projection of the meristem surface that minimizes the distortion of the distances between primordia. The local distortion of distances is equal to 1-cos θ where θ is the angle between the local normal to the surface and the normal of the plane onto which the surface is projected. It is possible to minimize the overall distortion by selecting a projection plane that coincides with the mean normal of the surface. We found that the projection error is everywhere less than 8% (Figure 7C). These observations support the modeling of the meristem as a flat disk. Ultimately, the reconstructed surface could be used in the simulations, but we do not pursue this direction here to keep the model as simple as possible.

The Ontogenetic Graph of a Pattern

The locations of the primordia centers (Figures 7 and 8) were collected using a computer-assisted user interface. The representation of the pattern in terms of the Voronoi tessellation and the Delaunay triangulation (Figure 8C) offers a possible basis for comparing observed and simulated patterns. Moreover, the inclusion of one additional piece of information can help account for the developmental history or ontogenesis of the pattern. Given an iterative process in which primordia are initiated centripetally around the meristem, we call the *parents* of a primordium its two closest older neighboring primordia, that is, the two closest primordia located radially away from a given primordium (Figure 8B). The directed graph formed by joining each primordium to its parents is the *ontogenetic graph* of the pattern (Figure 8B). It records both the topology and the ontogenesis of the pattern. The ontogenetic graph is a subgraph of the Delaunay triangulation (compare Figure 8B and 8C). Typically, it corresponds to the parastichies of the pattern, but, although it can be hard to define parastichies in non-lattice patterns, it is always possible to define their ontogenetic graph. Therefore, the ontogenetic graph is a robust and succinct way of describing a phyllotactic pattern.

Comparison of Observed and Simulated Patterns

We now consider two ways to compare a pattern extracted from a meristem micrograph (pattern A) and a simulated pattern (pattern B) whose outer boundary is a primordia front F of pattern A. The first approach presupposes that the Voronoi

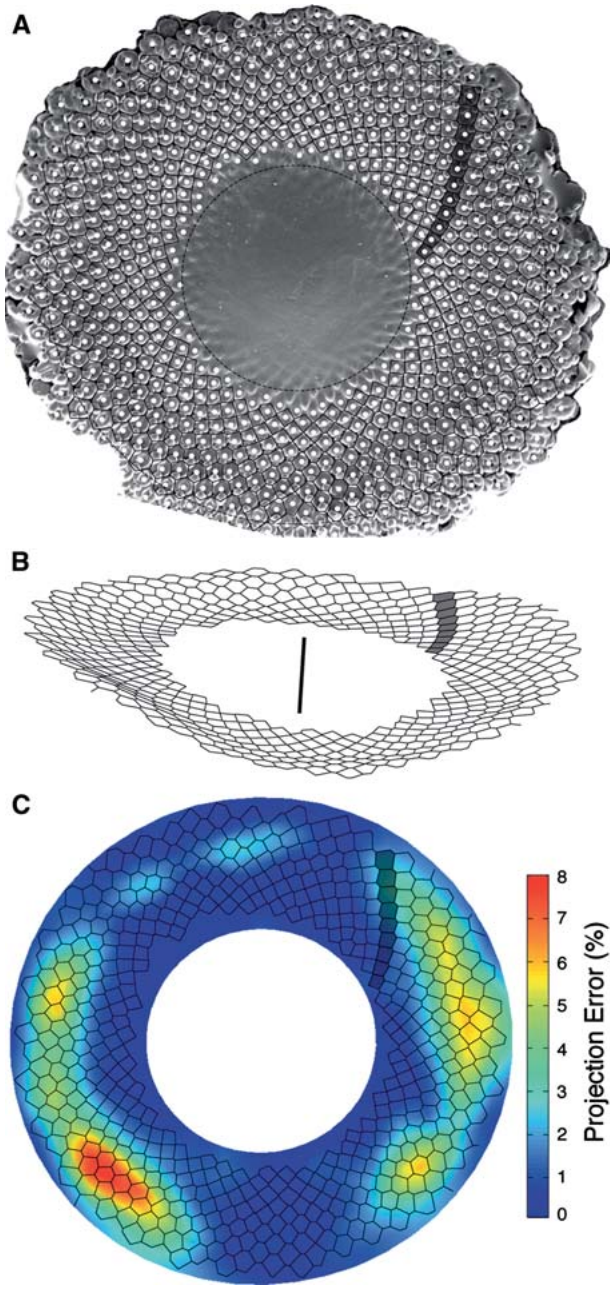

Figure 7. Reconstruction of the sunflower capitulum. (**A**) Two concentric circles indicate the region of the capitulum that was reconstructed. Polygons represent the Voronoi cell of the primordia. The second stereoimage of the meristem is not shown. (**B**) Side-view of the reconstructed surface. (**C**) Top-view of the capitulum. The Voronoi cells computed from the floret positions are drawn in black. The color map shows the error associated with the projection of a 3-D surface onto a plane. The same (parastichy has been highlighted in all three panels.

inscribed circles of B overlap those of A in a one-to-one fashion in some region of A. Given this one-to-one correspondence, we can quantify the degree of

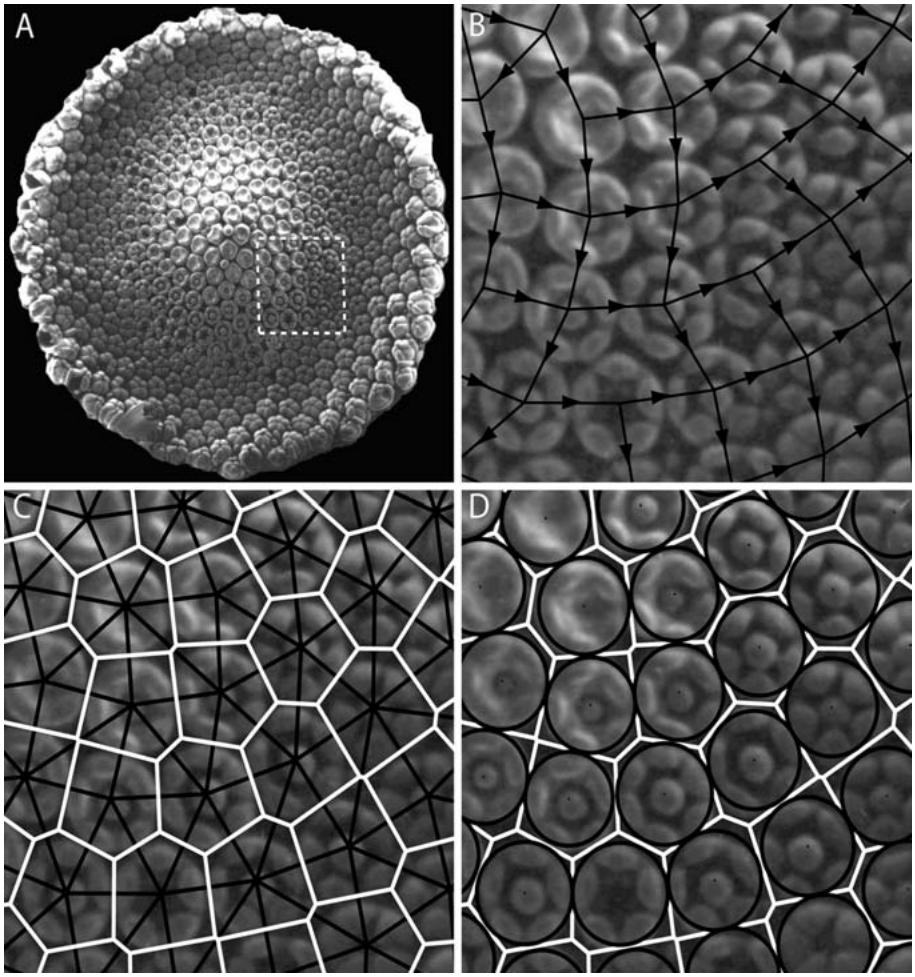

Figure 8. Ontogenetic graph, Voronoi cells and Delaunay triangulation for an artichoke capitulum. Panels **B, C,** and **D** depict the same magnified region shown in **A**. (**A**) Entire capitulum. (**B**) Ontogenetic graph, a subset of the Delaunay triangulation shown in **C**. The initiation of flower primordia proceeded approximately from the lower right corner of the panel to the upper left corner. Arrowheads show the local direction of the graph. Edges leaving a primordium point to the parents of that primordium. (**C**) The Voronoi cells (white) and Delaunay triangulation (black) of the pattern. (**D**) Voronoi inscribed circles. Note that the small spheres at the center of many flowers are small air bubbles that were trapped when the mould was made.

overlap using the following dimensionless measure of fit. If P_A is a target primordium overlapped by P_B with respective radii R_A and R_B, we define the *percent relative fit* (*PRF*) as:

$$PRF = \left(1 - \frac{dist(P_A, P_B)}{R_A + R_B}\right) 100\%$$

Note that *PRF* = 100% when the centers coincide and *PRF* = 0% when the circles representing the primordia are tangent. Finally, *PRF* is negative when the primordia are disjoint. The second approach is to compare the topologies of the ontogenetic graphs of B and A. The distance between these graphs can be measured by computing the minimal number of edge substitutions that transforms one graph into the other.

We analyzed the geometry of the capitula of one artichoke and one sunflower using the methods described above. Both have parastichy numbers 34, 55 (with dislocations in the center for the artichoke). Approximating the primordia by the Voronoi inscribed circles, it is possible to plot the primordium radii as a function of the distance to the meristem center (centroid of the data) (Figures 9D and 10D). One observes a marked difference in the slopes of the linear fits: the slope in the sunflower data is three times higher than that for the artichoke. The small variation in primordium size in the artichoke indicates that it is close to a constant radius mode. The ontogenetic graph of the sunflower near the meristem is topologically equivalent to that of a spiral lattice; that is, all interspaces are rhombic (Figure 10C). Because lattice patterns are possible only within the constant ratio mode, we have used this model to simulate the sunflower.

We ran 200 iterates with initial conditions given by the fronts seen in Figures 9 and 10. Parameters were (roughly) optimized so as to give the best fit in both cases. It was possible to achieve a better fit for the artichoke case than for the sunflower case. There was a one-to-one overlap for all 200 iterates for the artichoke. For the sunflower, the one-to-one criterion was satisfied until iterate 195, where the

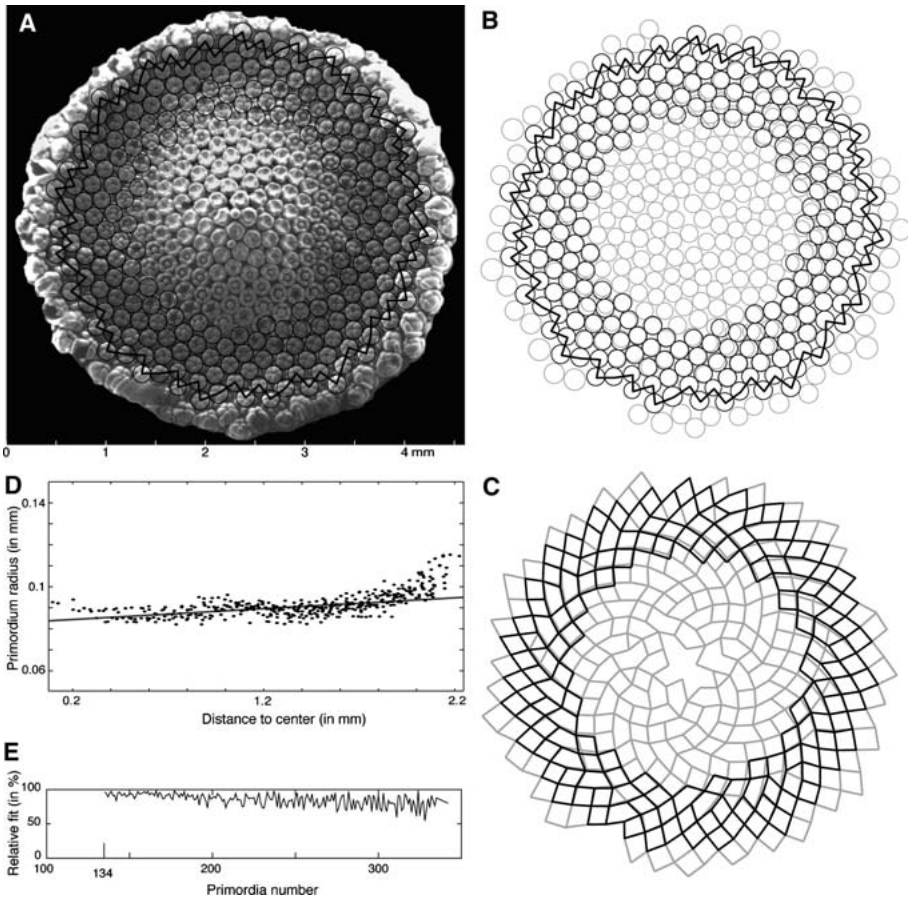

Figure 9. Dynamical simulation on an artichoke capitulum using constant radius $r = 0.095$ mm, 150 iterates are shown. (**A**) SEM of the capitulum with simulated primordia superimposed in black. The initial front is represented by a black zigzagging loop. (**B**) Same information as in A with the primordia of the artichoke represented by the Voronoi inscribed circles (in gray). (**C**) The ontogenetic graph of the simulation (black) superimposed to that of the data (gray). (**D**) Graph of primordium radius vs. distance to the center, shown in same scale ratio as Figure 10D. The slope of the linear fit is 0.0075. (**E**) Graph of the Percent Relative Fit of the n^{th} primordium and the simulated primordium that overlaps it. Primordia were ordered according to decreasing distance from center. The radius r was chosen to maximize the *PRF*.

simulated primordium landed on a site already overlapped. We found a mean *PRF* of 85.3% for the artichoke and of 78.5% for the sunflower. However, restricted to the last 100 iterates, the mean *PRF* was 81.3% for the artichoke, but only 68.2% for the sunflower.

As expected, the Voronoi circles seem to underestimate the primordia size, as indicated by the optimal radius for the dynamics. This discrepancy is much more significant in the sunflower than in the artichoke. Indeed, the Voronoi radius is 93% of the optimal radius in the artichoke. In the sunflower this percentage is 63%. We suspect that the discrepancy in the sunflower is amplified by the marked elliptical shape of the young primordia.

Discussion

The phyllotactic patterns observed in plants are based on a few standard types, with the Fibonacci type patterns being predominant. Curiously, the commonly observed plant patterns are but a small fraction of a much larger universe of patterns (Figure 3) (van Iterson 1907). (For an interactive exploration of the universe of spiral lattices, see www.math.smith.edu/phyllo/Applets.) Why, then, have plants adopted some specific patterns? This central question served as the motivation for our work. This article offers a framework and numerical methods to compare the patterns observed in Nature with those generated by simple dynamical systems. At the center of the comparison is the concept of ''ontogenetic graph'' which records the developmental history of a pattern. The comparison is supported by a set of tools and ancillary concepts both at the experimental level and the theoretical level.

We have shown that two geometrical dynamical systems based on the hard disk assumption can account for the patterns observed in the inflorescence of asteraceae. For this work, we deliberately selected meristems with nearly flat geometries so that simpler dynamical systems could be used. The simplicity of the models is a great advantage because the dynamical systems can be studied in detail to probe the universe of all phyllotactic patterns. We performed such an analysis previously in the cylindrical geometry (Atela and others 2002).

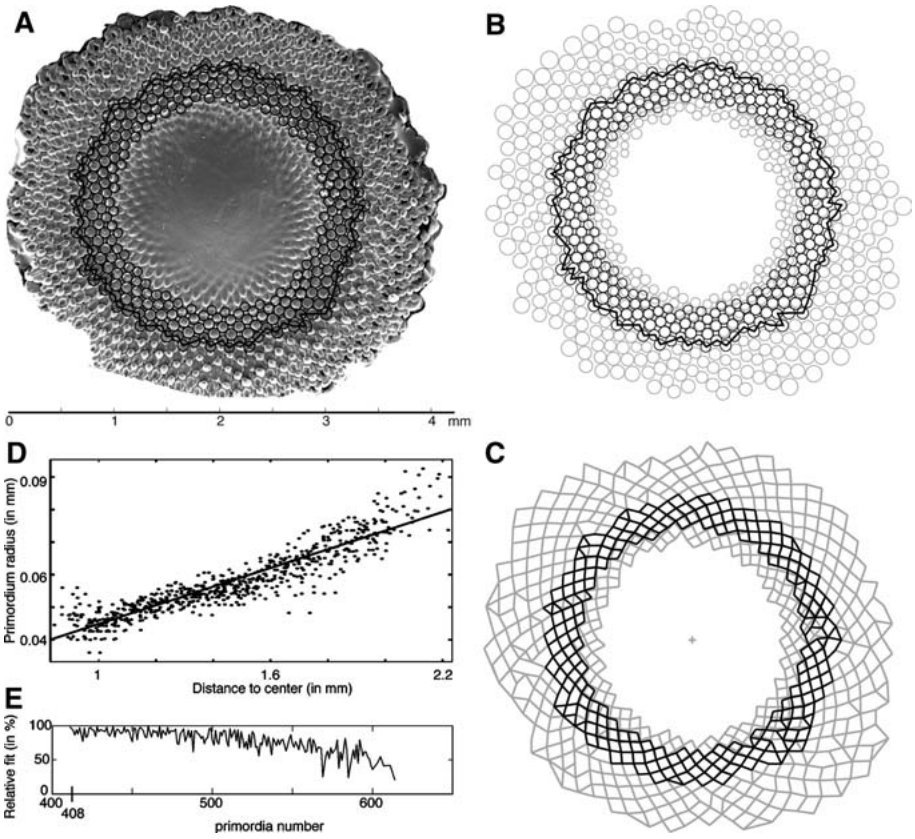

Figure 10. Simulation study on a sunflower capitulum with constant ratio $\Gamma = 0.0444$ and 200 iterates. (**A**) SEM of the capitulum with simulated primordia superimposed in black. The initial front is represented by a black zigzagging loop. (**B**) Same information, with the primordia of the sunflower represented by the Voronoi inscribed circles (in gray). (**C**) Ontogenetic graphs of the simulation (black) and data (gray) superposed. (**D**) Graph of primordium radius vs. distance to center, shown in same scale ratio as Figure 9D. The slope of the linear fit is 0.028. (**E**) Graph of the Percent Relative Fit of the n^{th} primordium and the simulated primordium that overlaps it.

Although many articles have emphasized the similarity between observed and simulated patterns, there are relatively few instances where an explicit one-to-one comparison was performed. Couder (1998) directly compared the location of leaves along sunflower stems with simulations obtained from the computer model he helped develop (Douady and Couder 1996). Good agreement was achieved between the data from many specimens and the computer simulations. Another comparison of a dynamical model to a phyllotactic pattern was performed by Battjes and Prunsikiewicz (1998). The floret patterns in *Microseris pigmaea* inflorescences were simulated by a collision disk model. This model places congruent disks with a divergence angle equal to the golden angle and readjusts their positions to find the closest tangent fit to the older ones. As mentioned by the authors, the initial angular bias reduces the generality of the approach, but otherwise the model bears many similarities to our constant radius model.

From Hard Disks to Squishy Biology

It may seem paradoxical at a time when great strides are being made in our understanding of the molecular and cellular basis of phyllotaxis that geometrical models of this process are used instead of mechanistic ones. The developmental rules implemented in the geometrical model are taken to be ''downstream'' consequences of the molecular and cellular controls of primordium initiation. The advantages of operating at a slightly more abstract level are many. First, although detailed mechanistic models can reproduce some phyllotactic patterns, their complexity is such that the analysis of their morphogenetic potential must be performed numerically. To understand fully how the positioning of new primordia creates the classic plant patterns, models of greater simplicity are required because they allow a detailed analysis of the universe of patterns accessible to them. Second, several distinct mechanistic models have been shown to reproduce plant-like patterns. Therefore, there is not a unique mechanistic model to study. Many experiments are required before the validity of the current mechanistic models can be ascertained.

The type of interactions implemented in our models (that is, the hard disk assumption) may seem *a priori* quite remote from the type of interactions likely to be at work in the meristem. We believe, however, that simple developmental rules may emerge from the common molecular and cellular controls invoked for phyllotaxis. In particular,

the diffusion and transport of auxin from cell to cell may very well be compatible, at a larger scale, with the simple spacing rule embodied in the hard disk assumption. Perhaps the most important contribution of geometrical models is to reduce complex phyllotactic patterns to a set of local rules that are repeated recursively. These local rules, rather than the overall patterns, are ultimately what needs to be explained at the mechanistic level.

ACKNOWLEDGMENTS

This work was supported in part by National Science Foundation (NSF) collaborative grant 0540740 to P.A. and C.G., and collaborative grant 0540662 to J.D. We acknowledge Smith College for additional funds to support V.J. and J.W., and the Mellon Foundation for supporting exchange travels of the senior authors. Finally, we thank the Center for Nanoscale Systems (Harvard) for use of their imaging facilities.

REFERENCES

Adler I. 1998. Generating phyllotaxis patterns on a cylindrical point lattice In: Jean RV, Barabé D editors. *Symmetry in Plants* Singapore: World Scientific. pp. 249–279.

Atela P, Golé C, Hotton S. 2002. A dynamical system for plant pattern formation: a rigorous analysis. J Nonlinear Sci 12:641—676.

Atela P, Golé C. 2006. New concepts in phyllotaxis: multilattices and primordia fronts, in preparation.

Battjes J, Prusinkiewicz P. 1998. Modeling meristic characters in asteracean flowerheads In: Jean RV, Barabé D. editors. *Symmetry in Plants* Singapore: World Scientific. pp. 281–312.

Bravais L, Bravais A. 1837. Essai sur la dispositions des feuilles curvisériées. Ann Sci Nat Bot 7, deuxième série: 42–110.

Couder Y. 1998. Initial transitions, order and disorder in phyllotactic patterns: the ontogeny of *Helianthus annuus*, a case study. Acta Soc Bot Pol 67:129–150.

Douady S. 1998. The selection of phyllotactic patterns In: Jean RV, Barabé D. editors. *Symmetry in Plants* Singapore: World Scientific. pp. 335–358.

Douady S, Couder Y. 1996. Phyllotaxis as a dynamical self organizing process (Part I, II, III). J Theor Biol 139:178–312.

Dumais J, Kwiatkowska D. 2002. Analysis of surface growth in shoot apices. Plant J 31:229–241.

Erickson RO. 1973. Tubular packing of spheres in biological fine structure. Science 181:705–716.

Grandjean O, Vernoux T, Laufs P, Belcram K, Mizukami Y, and others. 2004. In vivo analysis of cell division, cell growth, and differentiation at the shoot apical meristem in *Arabidopsis*. Plant Cell 16:74–87.

Hein LRO, Silva FA, Nazar AMM, Ammann JJ. 1999. Three-dimensional reconstruction of fracture surfaces: area matching algorithms for automatic parallax measurements. Scanning 21:253–263.

van Iterson G. 1907. Mathematische und Mikroskopisch-Anatomische Studien über Blattstellungen nebst Betraschtungen über den Schalenbau der Miliolinen. Gustav Fischer, Jena, Germany.

Koch AJ, Bernasconi G, Rothen F. 1998. Phyllotaxis as a geometrical and dynamical system In: Jean RV, Barabé D. editors. *Symmetry in Plants* Singapore: World Scientific. pp. 459–486.

Kunz M. 1997. Ph.D. Phyllotaxie, billards polygonaux et theorie des nombres (Thesis). Université de Lausanne, Switzerland.

Kwiatkowska D, Dumais J. 2003. Growth and morphogenesis at the vegetative shoot apex of *Anagallis arvensis* L. J Exp Bot 54:1585–1595.

Levitov LS. 1991. Energetic approach to phyllotaxis. Europhys Lett 14:533–539.

d'Ovidio F, Mosekilde E. 2000. Dynamical system approach to phyllotaxis. Phys Rev E 61:354–365.

Palmer JH, Steer BT. 1985. The generative area as the site of floret initiation in the sunflower capitulum and its integration to predict floret number. Field Crops Res 11:1–12.

Piazzesi G. 1973. Photogrammetry with the scanning electron microscope. J Phys E: Sci Instr 6:392–396.

Reddy GV, Heisler MG, Ehrhardt DW, Meyerowitz EM. 2004. Real-time lineage analysis reveals oriented cell divisions associated with morphogenesis at the shoot apex of *Arabidopsis thaliana*. Development 131:4225–4237.

Reinhardt D, Mandel T, Kuhlemeier C. 2000. Auxin regulates the initiation and radial position of plant lateral organs. Plant Cell 12:507–518.

Reinhardt D, Frenz M, Mandel T, Kuhlemeier C. 2003a. Microsurgical and laser ablation analysis of interactions between the zones and layers of the tomato shoot apical meristem. Development 130:4073–4083.

Reinhardt D, Pesce ER, Stieger P, Mandel T, Baltensperger K, and others. 2003b. Regulation of phyllotaxis by polar auxin transport. Nature 426:255–260.

Rivier N, Occelli R, Pantaloni J, Lissowski A. 1984. Structure of Bénard convection cells, phyllotaxis and crystallography in cylindrical symmetry. J Physique 45:49–63.

Rothen F, Koch AJ. 1989. Phyllotaxis, or the properties of spiral lattices. I. Shape invariance under compression. J Physique 50:633–657.

Schwabe WW, Clewer AG. 1984. Phyllotaxis—a simple computer model based on the theory of a polarly-translocated inhibitor. J Theor Biol 109:595–619.

Snow M, Snow R. 1932. Experiments on phyllotaxis. II—the effect of displacing a primordium. Phil Trans R Soc Lond 222:353–400.

Williams MH, Green PB. 1988. Sequential scanning electron microscopy of a growing plant meristem. Protoplasma 147:77–79.

Williams RF, Brittain EG. 1984. A geometrical model of phyllotaxis. Aust J Bot 32:43–72.